Full Paper Word template for IMSD 2018

X. Liu, V.L. Markine and Y. Ma

Section of Railway Engineering, Delft University of Technology,
Corresponding author: v.l.markine@tudelft.nl

ABSTRACT — *The paper presents the results of comparison of the multibody system (MBS) and explicit finite element (FE) models for analysis of wheel-rail interaction in railway crossings. The vehicle-crossing MBS model is developed in the commercial package VI-Rail. The FE model (LS-Dyna) of the crossing developed here uses the novel features specifically developed for the explicit FE analysis of wheel-rail interaction, such the adaptive mesh refinement procedure. Both models are parts of an integrated tool for analysis an improvement of performance of the railway crossings. The vehicle and track configurations in both models are adjusted to maximally match the real situation of the Dutch railway track. The simulation results have shown that some of the major dynamic responses, such as wheel impact location, wheel-rail contact forces and wheel vertical displacements, are comparable,*

1 Introduction

Railway turnouts are essential components that provide guidance for the trains to transfer from one track to another. The gap between wing rail and nose rail in the crossing panel makes the turnout crossing one of the weakest parts in the railway track. The studied type of crossings, which is a part of a double crossover, is the casted manganese steel crossing with the angle of 1:9 (Figure 1a-b). This type of crossings, which are quite common on the Dutch railway network, suffer very much from severe plastic deformation and cracks leading to the spalling damage or even to sudden fracture of the crossing nose (Figure 1c). These crossings are mainly passed in the main (facing or trailing) direction with relatively high speeds (140 km/h). The service life of such crossings in the Netherlands has become prohibitively short that in some cases is 1 year. Therefore, this type of crossings has been chosen here for comparison of the numerical models, that later will be used to analyse the poor performance of these crossings and to suggest the ways of its improvement.

There are several parameters, which can influence the wheel/crossing interaction, such as the cross-sectional geometry, material properties of the crossing rail, axle loads, wheel profile, vehicle velocity etc. Therefore, the numerical model should take into account the dynamic behaviour of both track and vehicle that can be achieved using the multi-body system (MBS) analysis. From such an analysis the main responses of the railway system like displacements, accelerations and forces can be obtained. However, the stress and strain results especially in the wheel-rail interface are not available from MBS analysis. In order to obtain these response quantities the (explicit) dynamic finite element (FE) model can be used that accounts for plastic deformation and hardening of the material on a local scale (wheel-rail contact).

However, such FEM simulations are significantly time consuming as compared to the MBS simulations and can hardly be used in the analyses where the multiple simulations are involved e.g. in the design improvement and optimisation. Therefore, in order to thoroughly study the performance of a railway crossing, both MBS and FE methods are necessary. It should be noted that for a fast analysis of turnout-vehicle interaction a 2-D model can be used as well [10].

In this study the dynamic analysis of the crossing performance is performed using both the MBS and FEM models. Prior to the simulations the input data of the models have been adjusted according to the analysed railway system. The results of the simulations are compared and discussed.

In the Section 2, the general description of the two numerical models is given. The comparison of the MBS and FEM results is performed in Section 3. Followed by the detailed FE-based contact solution presented in Section 4. Finally, concluding remarks are drawn in Section 5.

2 Numerical models

The numerical models are developed based on the 1:9 casted manganese crossing and the VIRM double deck train that are commonly used in Dutch railway network. The rail type is UIC54 E1, and the wheel type is S1002. The profiles of rail and wheel are given in the figure below.

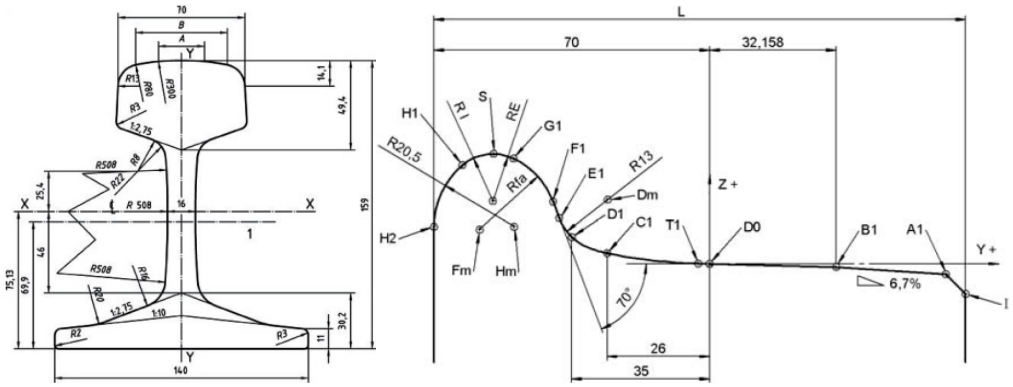

Figure 0-1: (a) UIC54 E1 Rail profile; (b) S1002 wheel profile

2.1 MBS vehicle – track model

The vehicle – crossing model developed in MBS methods is shown in Figure 0-2. The vehicle model is composed of the car body, the front bogie and the rear bogie, wherein the car body and bogie frames, as well as the wheelsets are treated as rigid bodies. The track model is a totally 60 m long straight line with a crossing section of 3.5 m. the rails are also treated as rigid bodies.

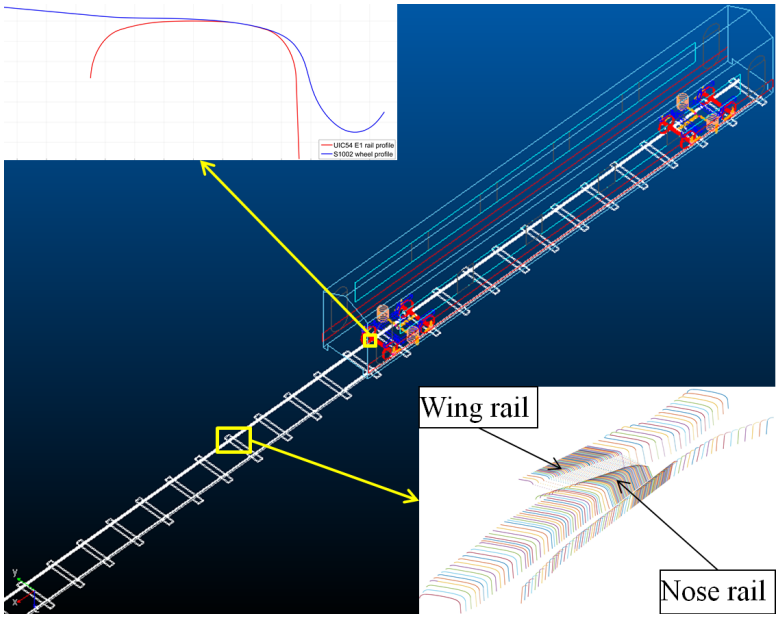

Figure 0-2: The MBS vehicle – crossing model

The number of points in the input rail profiles is restricted to maximum 500 points. In order to improve the accuracy, only the wheel-rail interaction part of the rail is taken into account.

2.2 FE wheel – crossing model

The wheel - crossing FE model is presented in Figure 0-3, wherein the length of the crossing is limited to 7.45 m. This finite length has been examined and confirmed in the previous research [1] that it is long enough to minimise the influence of the boundary conditions (at the two ends of the crossing rail) on the dynamic impact.

Only the solution regions where the wheel travels are discretized with fine mesh, leaving the remaining regions modelled with coarse mesh. Here, the solution region (fine mesh area) is an area to extract and analyse the contact properties, such as the resulting contact patch, normal pressure, shear stress, etc.

In this region, the mesh size is as small as 1.0 mm (See Figure 0-3a), which is prescribed for the purpose of capturing the accurate and high stress/strain gradients inside the contact patch. Moreover, the type of 3D 8-node brick (i.e., hexahedral) element (Solid164) with reduced (one point) integration is adopted so as to save the computational cost and enhance the robustness in cases of large deformations [11].

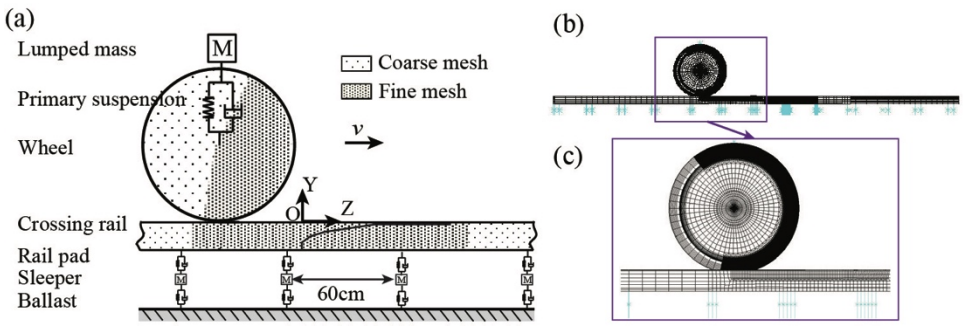

Figure 0-3: FE model of W/C dynamic impact: (a) Schematic of FE model; (b) FE model – global view; (c) FE model – close-up view.

The wheel is set to roll on the crossing rail from the origin of the global coordinate system O-XYZ over a short travelling distance of 1.2 m (See Figure 0-3a), which is long enough to ensure that the wheel can travel over the transition region completely. The initial train speed is 140 km/h. The rotations of the wheel around the Y-axis are disabled (i.e., turned off or prevented from occurring), since it is assumed that variations of the wheel-set's yaw angles are small over a short rolling distance (i.e., 1.2 m). More detailed FE modelling procedures/strategies are available in [12].

In the explicit FE simulations (ANSYS LS-DYNA), the penalty method is used to enforce the contact constrains, where a list of invisible "interface spring" elements are placed between all the penetrating slave segments and the master segments. Friction is based on the Coulomb formulation. More description on the contact algorithms can be found in [4].

2.3 Model parameters

For better comparison, the parameters and properties used in both models are checked prior the simulations, so that they represent the same real-life railway system.

The vehicle configurations of both models are given in Table 0.1. The axle load is 200 kN. In the FE model this is modelled by applied a corresponding lumped mass to the wheel, while in the MBS model, the total axle load is resulted from the wheelset, bogie and car body masses.

Table 0.1: Vehicle/wheelset configuration

Items		FE Model	MBS model
Wheel	Profile	S1002	
	Radius, m	0.46	
Wheelset	Mass, kg	1100	1700
Bogie	Mass, kg	18900	2600
Car body	Mass, kg	-	68000

It should be noted that in FE model, the lateral DOF is prescibed to zero.

Table 0.2: Track configuration

Track components		FE model	MBS model
Rail	Young modulus, GPa	210	
	Shear modulus, GPa	21	-
	Yield stress, MPa	480	-
	Mass density, kg/m^3	7900	
Rail pad	Vertical stiffness, MN/m	1300	
	Vertical Damping, kN·s/m	45	
	Lateral stiffness, MN/m	-	280
	Lateral Damping, kN·s/m	-	58
	Roll stiffness, MN/m	-	360

	Roll Damping, kN·s/m	-	390
Ballast	Vertical stiffness, MN/m	45	
	Vertical Damping, kN·s/m	32	
	Lateral stiffness, MN/m	-	45
	Lateral Damping, kN·s/m	-	32

Both FE model and MBS simulation concentrate on the interaction between wheel and rail as the wheel/vehicle passes the crossing part of the turnout.

3 Comparisons of FE and MBS results

A detailed comparison between the field measured and FE simulated accelerations is performed after the simulations. In these simulations, the time step in MBS analysis is adjusted to the output results time step of the FE model.

To compare the results the following response quantities have been used:

- The transition region, defined by the location of the last contact on the wing rail and the first contact point in the crossing nose.
- The vertical and the lateral coordinates of the wheel trajectory.
- The contact force between the wheel and rail.
- The contact pressure between the wheel and rail

The first two responses are related to the global responses of the models and characterise the correctness of the geometry representation in the models, while the last two are related to the local properties and describe the modelling of the wheel-rail contact. In the MBS results the results from the first wheelset of the vehicle is used.

3.1 Transition region

The results of the comparison of the transition region in both model is shown in Figure 0-4(a). The transition region, defined as the two-points contact section in the MBS model, is between 184 mm and 215 mm.

In comparison to the MBS results, the transition region predicted by the FE simulations, starts at 180 mm and ends at 223 mm as shown in Figure 0-4(b). It should be noted that in the FE model the plastic deformations region on the wing rail and the crossing nose, that are shown in the legend in Figure 0-4(b).

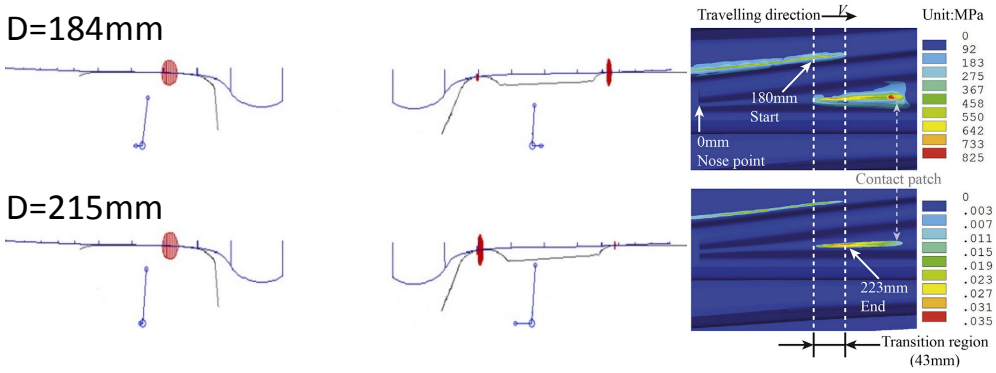

(a) (b)

Figure 0-4: Comparison of transition region: (a) MBS results; (b) FE results.

By comparing these results it can be concluded that the transition regions in both models are very close to each other. The differences might result from the differences in contact detection/definition in the MBS and FE models.

The simulation results have also been compared with the measurement results as shown in Figure 0-5. The transition regions obtained in the simulations are shown with green (MBS) and red (FEM) lines.

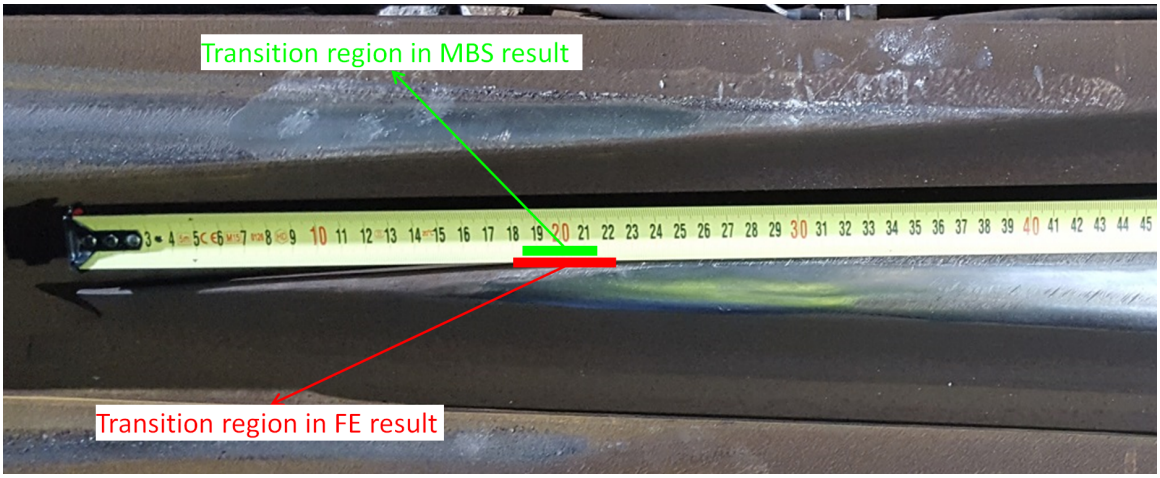

Figure 0-5: Transition region field observations

As it can be seen from this figure, both regions are located in the transition zone on the crossing defined by the shining areas on the wing rail and crossing nose. The transition zone on the crossing is larger than the ones obtained in the simulations, which can be explained by the ideal initial conditions (zero lateral displacements) of the wheels used in the simulations and absence of the rail/wheel irregularities. In reality, every wheel passes the crossing with certain angle and lateral shift that results in earlier/later contact in the transition region. The fact that the simulated transition region is included in the transition region of the real crossing proves the correctness of the simulation results.

3.2 Wheel trajectory

Figure 0-6 and Figure 0-7 shows respectively the vertical and lateral trajectories of the wheel in the MBS and FEM simulations.

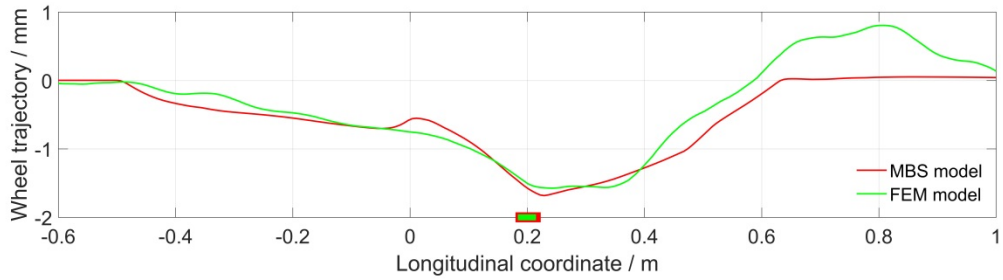

Figure 0-6: Vertical wheel trajectory.

As it can be seen from these figure the vertical trajectories are pretty close, while the lateral trajectories are slightly, which can be explained by the fact that the lateral displacements in the FEM model were prescribed to zero.

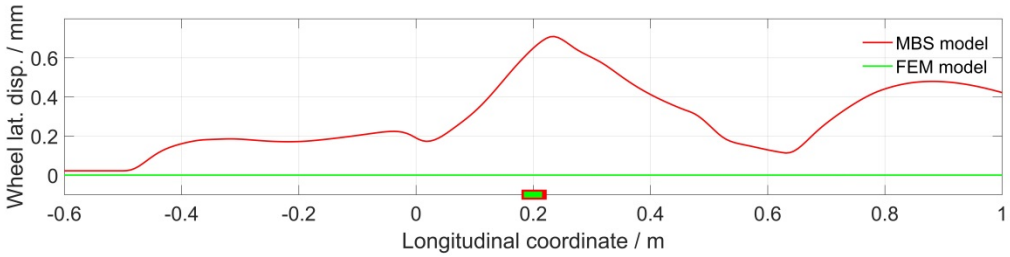

Figure 0-7: Comparison of wheel lateral displacement.

Based on these results it can be concluded that both models describe the same real-life system.

3.3 Forces results

Figure 0-8 shows the comparison of the contact forces obtained from MBS and FE simulations. Figure 0-9 shows the comparison of contact pressure. The contact pressure is obtained as the normal contact force divided by the corresponding contact area.

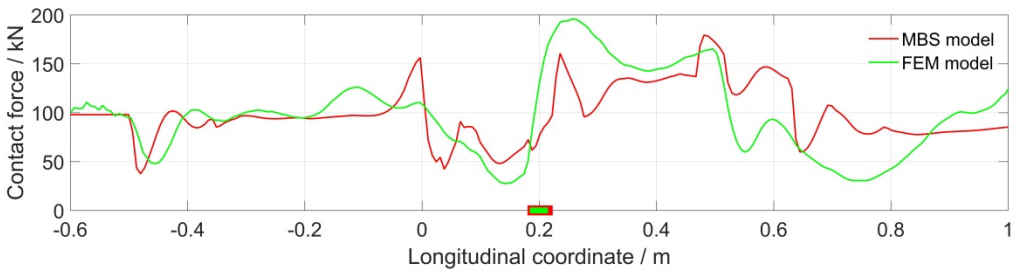

Figure 0-8: Comparison of contact forces.

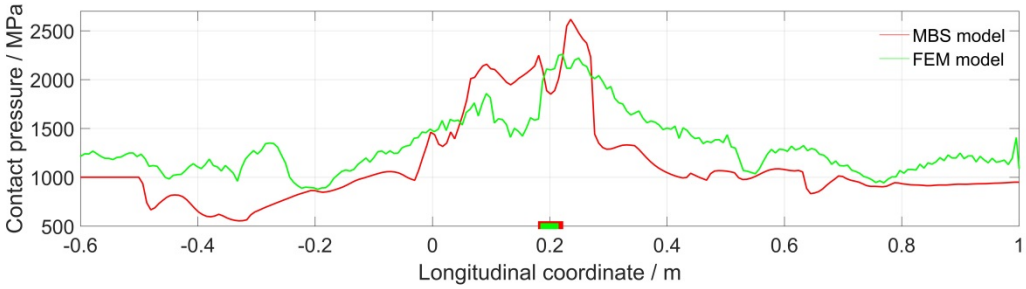

Figure 0-9: Comparison of contact pressure.

From these figures it can be concluded that the results are very much comparable. The differences can result from the differences in the models such as one wheel in the FEM model and wheelset and vehicle in the MBS model, prescription of the lateral displacements in FEM model. Also the differences in the contact analysis methods implemented in both models contribute to the differences in these results.

4 Detailed FE contact solution

In this section, the detailed FEM results including both the surface and subsurface contact stresses are presented.

4.1 Normal pressure and Shear stresses

Figure 0-10 (a) shows the contour plots of the normal pressure distribution at the time point, when the maximum contact pressure occurs. It should be noted that the compressive pressure is treated as positive for better demonstration of the distribution of contact pressure.

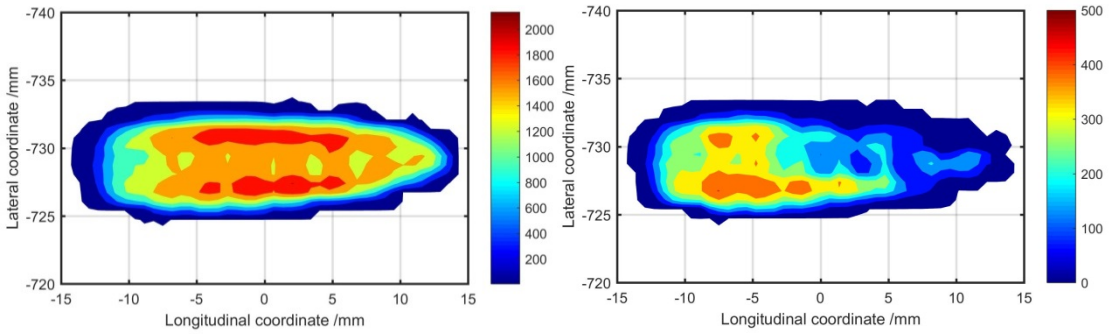

(a) (b)

Figure 0-10: (a) Normal pressure; (b) Shear stresses

4.2 Von-Mises stress

Generally, Von-Mises stress is adopted as a measure of material performance assessment under specific contact conditions for elastoplastic material.

Figure 0-11 shows the variation of Von-Mises stress during the whole time history. The most critical moment, when the Von-Mises stress reaches peak value is the one at the distance of 223 mm.

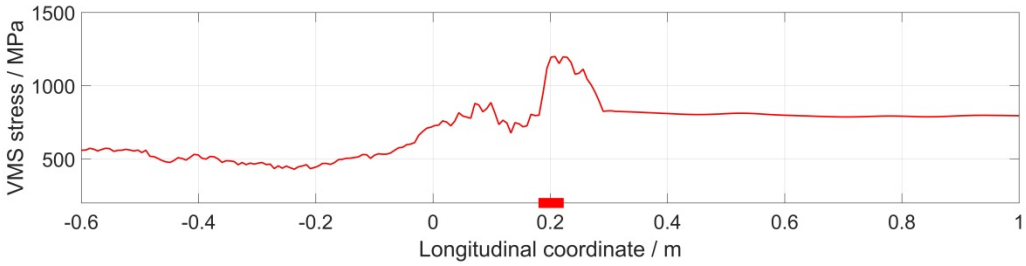

Figure 0-11. Variation of VMS stress during the whole time history.

It is observed that the maximum Von-Mises stress of 1197 MPa is far above the yield limit (480 MPa, See Table 0.2) of the materials. Such a high stress concentration is attributed to the relatively small size of the contact patch as well as the amplified impact loads (See Figure 0-8).

Figure 0-12 shows that the maximum Von-Mises stress is concentrated at a small volume of material, which is ranging from the rail top surface to 2.0 mm beneath.

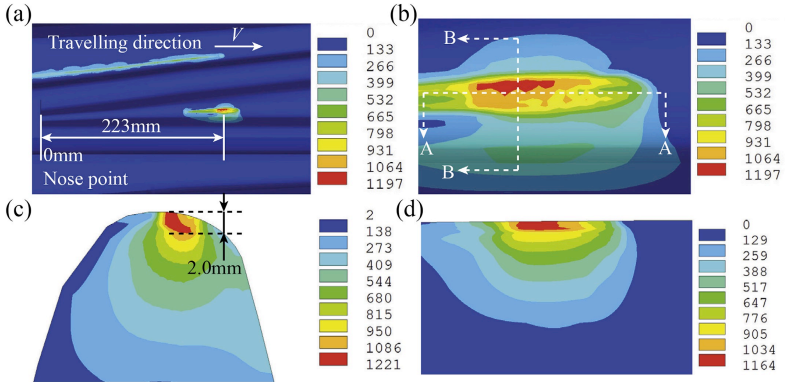

Figure 0-12. Distribution of maximum VMS stress at a time-point selected: (a) Global view; (b) Close-up view; (c) Von-Mises stress on cutting plane “BB”; (d) Von-Mises stress on cutting plane “AA”.

5 Conclusions

In this paper the dynamic performance of the 1:9 railway crossing is analysed by using both MBS and FEM models, which were validated in the previous studies. Prior to the simulations the models and their parameters have been adjusted so that they describe the same real life system.

Based on the results and discussions, the following conclusions are drawn:

- The displacement results such as the transition region and the wheel trajectory of MBS and FEM models are close to each other.
- Moreover, the transition regions are within the transition region observed on the real crossing, that proves the correctness of the results

- The forces results are close as well. The differences can be due the differences in the models such as one wheel in the FEM model and wheelset and vehicle in the MBS model, prescription of the lateral displacements in FEM model. Also the differences in the contact analysis methods implemented in both models contribute to the differences in these results.

The detailed FE contact solution obtained using MBS has revealed the stress distribution in the crossing nose and can indicate the location of the potential damage initiation.

References

[1] C. Wan, V.L. Markine, I.Y. Shevtsov, Improvement of vehicle–turnout interaction by optimizing the shape of crossing nose, Vehicle System Dynamics, 52, 1517-1540, 2014.

[2] Ma, Y., Mashal, A. A., & Markine, V. (2018). Modelling and experimental validation of dynamic impact in 1:9 railway crossing panel. *Tribology International*, *118*, 208-226. DOI: 10.1016/j.triboint.2017.09.036

[3] V. L. Markine and I. Y. Shevtsov, (2013) An Experimental Study on Crossing Nose Damage of Railway Turnouts in The Netherlands, presented at the *Proceedings of the Fourteenth International Conference on Civil, Structural and Environmental Engineering Computing* (CC2013), 2013.

[4] Liu, X, Markine, VL & Shevtsov, I (2015). Performance study of a double crossover for facing and trailing directions. In M Rosenberger, M Plochl, K Six & J Edelmann (Eds.), *Proceedings of the 24th international symposium on dynamics of vehicles on roads and tracks, IAVSD 2015* (pp. 1-9). Boca Raton: CRC Press.

[5] V.L. Markine, C. Wan, (2016) Performance Optimised Geometry of Railway Crossings: Design and Implementation, *International Journal of Railway Technology*, 5(2), 1-25, 2016. doi:10.4203/ijrt.5.2.1

[6] Liu, X, Markine, VL & Shevtsov, I (2016). A performance study of railway crossings in facing and trailing directions. In J Pombo (Ed.), *Proceedings of the 3rd international conference on railway technology: Research, development and maintenance* (pp. 1-10). Stirlingshire: Civil-Comp Press.

[7] M. Wiest, E. Kassa, W. Daves, J. C. O. Nielsen, and H. Ossberger, "Assessment of methods for calculating contact pressure in wheel-rail/switch contact," *Wear,* vol. 265, pp. 1439-1445, 10/30/ 2008

[8] Ma, Y, Mashal, AA & Markine, VL (2016). Numerical analysis of wheel-crossing interaction using a coupling strategy. In J Pombo (Ed.), *Proceedings of the 3rd international conference on railway technology: Research, development and maintenance* (pp. 1-19). Stirlingshire: Civil-Comp Press.

[9] A. A. Mashal, "Analysis & Improvement of railway crossing using explicit finite element method," MSC thesis, Delft University of Technology, Delft, 2016, http://repository.tudelft.nl/.

[10] Markine, V.L., M.J.M.M. Steenbergen, and I.Y. Shevtsov, Combatting RCF on switch points by tuning elastic track properties. *Wear*, 2011. **271**(1-2): p. 158-167.

[11] J. Hallquist, "ANSYS/LS-DYNA Theoretical Manual [M]," Livermore Software Technology Corporation, USA, 2005.

[12] Y. Ma, A. A. Mashal, and V. L. Markine, "Modelling and experimental validation of dynamic impact in 1:9 railway crossing panel," Tribology International, vol. 118, pp. 208-226, 2018.

[13] Y. Ma, V. L. Markine, A. A. Mashal, and M. Ren, "Modelling verification and influence of operational patterns on tribological behaviour of wheel-rail interaction," *Tribology International,* vol. 114, pp. 264-281, 2017.